Phys. Status Solidi A **210,** No. 1, 226–229 (2013) / **DOI** 10.1002/pssa.201200403

physica status solidi a
www.pss-a.com
applications and materials science

Structural properties of SnO_2 nanowires and the effect of donor like defects on its charge distribution

M. Zervos*[,1], A. Othonos[2], D. Tsokkou[2], J. Kioseoglou[3], E. Pavlidou[3], and P. Komninou[3]

[1] Nanostructured Materials and Devices Laboratory, Department of Mechanical and Manufacturing Engineering, School of Engineering, University of Cyprus, P.O. Box 20537, 1678 Nicosia, Cyprus
[2] Research Center of Ultrafast Science, School of Physical Sciences, University of Cyprus, PO Box 20537, 1678 Nicosia, Cyprus
[3] Nanostructured Materials Microscopy Group, Department of Physics, Aristotle University of Thessaloniki, 54124 Thessaloniki, Greece

Received 20 June 2012, revised 22 November 2012, accepted 26 November 2012
Published online 24 December 2012

Keywords defects, nanowires, spectroscopy, tin oxide

* Corresponding author: e-mail zervos@ucy.ac.cy, Phone: 00357 22894509, Fax: 00357 22895081

Tin oxide (SnO_2) nanowires (NWs) with diameters of 50 nm, lengths up to 100 μm and a tetragonal rutile crystal structure have been grown by low pressure reactive vapour transport on 1 nm Au/Si(001). The free carrier density of the SnO_2 NWs measured by THz absorption spectroscopy was found to be $n = (3.3 \pm 0.4) \times 10^{16}\,cm^{-3}$. Based on this we have determined the one-dimensional (1D) sub-band energies, overall charge distribution and band bending via the self-consistent solution of the Poisson–Schrödinger equations in cylindrical coordinates and in the effective mass approximation. We find that a high density of 10^{18}–$10^{19}\,cm^{-3}$ donor-like defect related states is required to obtain a line density of 0.7×10^9 close to the measured value by taking the Fermi level to be situated ≈0.7 eV below the conduction band edge at the surface which gives a surface depletion shell thickness of 15 nm. We discuss the origin of the donor-like states that are energetically located in the upper half of the energy band gap as determined by ultrafast, time-resolved absorption–transmission spectroscopy.

1 Introduction Semiconductor nanowires (NWs) have been investigated intensively over the past decade in view of their potential application as emerging devices and the ongoing downscaling of integrated circuits (ICs) but also due to the upsurging interest in nanotechnology. Metal oxide (MO) semiconductor NWs are in particular attractive for the fabrication of sensors, solar cells, electronic and optoelectronic nanoscale devices. In the past we have investigated a broad range of MO NWs such as ZnO [1] In_2O_3 [2, 3] Ga_2O_3 [4] and SnO_2 NWs [5, 6]. The latter are attractive since they may be grown with uniform diameters of 50 nms and lengths up to 100 μm by the reaction of Sn with O_2 on Au/Si(001) thereby avoiding the incorporation of other impurities such as C which is included during carbothermal reduction synthesis of MO NWs. More importantly SnO_2 NWs do not grow on plain Si(001) via a self-catalytic mechanism like ZnO and Ga_2O_3. This permits selective area location growth on lithographically patterned Au on Si(001) via a vapour–liquid–solid (VLS) like mechanism [7]. Furthermore, indium tin oxide (ITO) NWs belong to the class of transparent conducting oxides which are useful for solar cells, displays and sensors [8–10]. However, an understanding of the fundamental properties of SnO_2 NWs and their dependence on defects is indispensable for their improvement and the realisation of high quality nanoscale devices.

Recently the effect of surface states on the position of the Fermi level in SnO_2 NWs was investigated by ultrafast pump–probe spectroscopy by Kar et al. [11] who used carbothermal reduction of SnO to prepare SnO_2 NWs and X-ray photoemission spectroscopy (XPS) to find the surface barrier height and depletion width using bulk-like analysis.

Here we show that ultrafast – time-resolved absorption–transmission spectroscopy is a powerful method by which we may determine the energetic position of mid-gap states related to defects but also the free carrier density in SnO_2 NWs *i.e.* by THz absorption spectroscopy, which was found to be $n = (3.3 \pm 0.4) \times 10^{16}\,cm^{-3}$. Based on this we have determined the energetic position of the one-dimensional

(1D) sub-bands, their occupancies but also the overall charge distribution and band bending via the self-consistent solution of the Poisson–Schrödinger equations in cylindrical coordinates and in the effective mass approximation. We find that a high density of 10^{18}–10^{19} cm^{-3} donor-like defect states is required to obtain a line density of 0.7×10^9 close to the measured value by taking the Fermi level to be situated ≈0.7 eV below the conduction band edge at the surface which gives a surface depletion shell thickness of 15 nm for a 50 nm diameter SnO_2 NW. We discuss the origin of the donor-like states and the critical dependence of the carrier density on the surface charge and potential.

2 Experimental methods SnO_2 NWs were grown using a low pressure chemical vapour deposition (LPCVD) reactor consisting of four mass flow controllers and a 1″ horizontal quartz tube (QT) furnace capable of reaching 1100 °C which was fed via a microflow leak valve that was positioned upstream just after the gas manifold. A chemically resistant, rotary pump capable of reaching 10^{-4} mBar was connected downstream.

For the growth of SnO_2, Sn (Aldrich, 2–14 Mesh, 99.9%) was weighed with an accuracy of ±1 mg. Square pieces of p^+ Si(001) ≈ 7 mm × 7 mm were cleaned sequentially in trichloroethylene, methanol, acetone, isopropanol, rinsed with de-ionised water, dried with N_2 and coated with Au having thicknesses of ≈0.5–20 nm by sputtering using Ar at 1×10^{-2} mbar.

After loading 0.2–1.0 g of Sn and the Au/p^+Si(001) samples into a ceramic boat the latter was inserted into the 1″ QT, which was subsequently pumped down to 10^{-4} mbar. Then the 1″ QT was purged with 600 sccm Ar for 10 min at 1 mbar after which the temperature was ramped to $T_G = 800$ °C at 30 °C min^{-1} using the same flow of Ar. Upon reaching 800 °C a flow of 10 sccms O_2 was added to the flow of Ar in order to grow the SnO_2 NWs over 60 min after which the reactor was allowed to cool down slowly for at least 30 min without changing the gas flows. The sample was always removed when the temperature was lower than 100 °C and the 1″ QT was changed regularly in order to maintain a clean, high temperature, zone for the growth of NWs.

The morphology of the SnO_2 NWs was examined with a TESCAN scanning electron microscope (SEM) while their crystal structure and phase purity were determined using a SHIMADZU, XRD-6000, X-ray diffractometer with Cu-Ka source, by performing a scan of θ–2θ in the range between 10° and 80°. Elemental analysis was performed by energy dispersive X-ray spectroscopy (EDXS) using a JEOL JSM 6390 SEM equipped with an Oxford EDS-WDS analyzer while cross-section transmission electron microscopy (XTEM) and high-resolution TEM (HRTEM) observations were carried out in a 200 kV JEOL 2011 electron microscope with a point resolution of 0.194 nm and a spherical aberration coefficient $C_s = 0.5$ mm. Samples for XTEM observations were prepared by the standard sandwich technique. Mechanical grinding of the samples was followed by low-voltage Ar^+ precision ion-milling (Gatan PIPS) to achieve electron transparency.

Finally SnO_2 NWs were harvested by ultrasonic vibration in isopropanol (IPA) and transferred by drop casting onto quartz for the purpose of carrying out ultrafast, time-resolved absorption–transmission spectroscopy and THz absorption described in detail elsewhere [5, 6].

3 Results and discussion The reaction of Sn with O_2 over the Au/Si(001) surface at 800 °C and 1 mbar lead to a high yield, uniform growth of SnO_2 NWs with diameters of 50 nm and lengths of many tens of μm which appeared as a white deposit on Si(001). A typical SEM image of the SnO_2 NWs is shown in Fig. 1(a). These exhibited clear peaks in the XRD shown as in Fig. 1(b) corresponding to the tetragonal rutile crystal structure of SnO_2 while from EDX analysis we find that the SnO_2 NWs consist of 74% Sn and 26% O_2. The

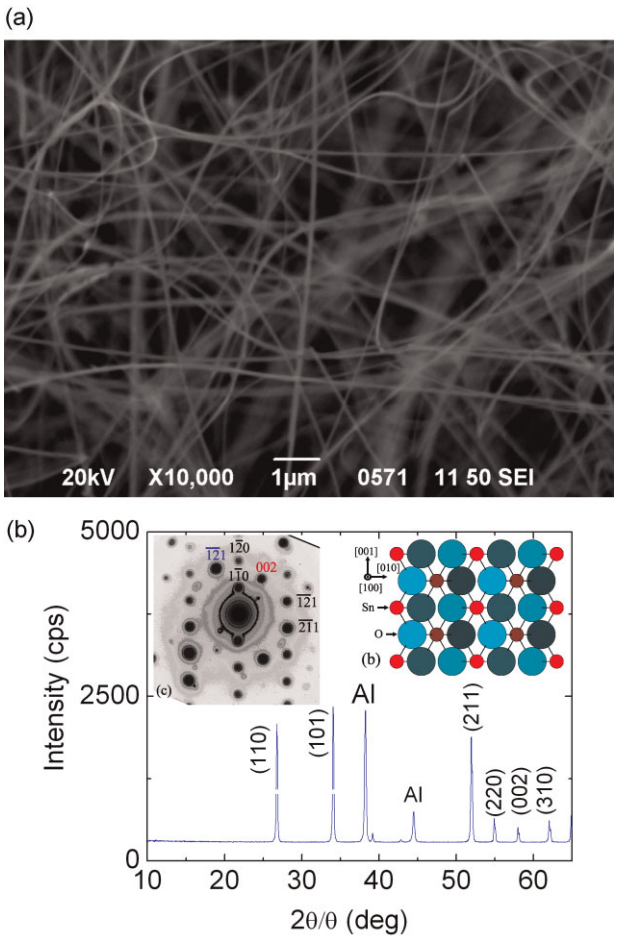

Figure 1 (online colour at: www.pss-a.com) (a) SEM image of SnO_2 NWs. (b) XRD spectrum of the SnO_2 NWs. The inset shows the atomistic model of the identified SnO_2 structure along [100]. Shading on atoms denotes different levels along the projection direction. Also shown as an inset the SAED taken along the [113] zone axis where the identified reflections are labelled. In red the 002 reflection of Au, in blue the $\overline{2}11$ reflection from a neighbouring NW.

SnO_2 NWs are Sn deficient or O_2 rich by about 4% while the Al peaks belonging to the holder are also identified.

From selected area electron diffraction (SAED) analysis in combination with HRTEM image simulations we determined that the structure of the SnO_2 NWs is the tetragonal rutile (space group: P42/mnm, lattice constants $a = 0.4738$ nm, $c = 0.31865$ nm) having dominant reflections of $\overline{2}11$, $1\overline{1}0$ and 020. The atomistic model of the identified SnO_2 structure projected along [100] is given as an inset in Fig. 1(b). The SAED pattern along the [113] zone axis is also shown as an inset in Fig. 1(b). It was recorded from neighbouring SnO_2 NWs and thus multiple $\overline{2}11$ reflections are detected. The 002 reflection (in red) of Au, used as catalyst, is also identified.

Images of the base of a SnO_2 NW on top of Si were obtained by HRTEM where the lattice fringes of the {020} SnO_2 planes (0.237 nm) were resolved. An amorphous interfacial area between SnO_2 NW and Si was also found. The top region of an NW showed lattice fringes of the {1–10} SnO_2 planes (0.335 nm). It should be noted that the amorphous like-interfacial area between the SnO_2 NWs and Si occurs most likely due to the lateral spread and coalescence of the SnO_2 NWs during the initial stages of growth which has been clearly shown when using hybrid polymer coated Au metal nanoparticles [7].

Ultrafast, time-resolved absorption–transmission spectroscopy, showed that there is a broad distribution of defect-related donor-like states in the upper half of the energy band gap as shown in Fig. 2(a) which is typical of other MO NWs such as Ga_2O_3[4, 5]. In particular we find that shallow-like states extend from 3.0 to 3.75 eV and deep-like donors from 2.0 to 2.8 eV above the valence band edge. These defect-related states are attributed to oxygen vacancies. A typical trace of the THz electric field versus time through the SnO_2 NWs transferred onto quartz is shown as an inset in Fig. 2(b). We find that the carrier density of the electrons in the SnO_2 NWs is $n = 3.3 \pm 0.4 \times 10^{16}\,\mathrm{cm}^{-3}$ by taking a Fourier transform of the electric field in the time-domain and then fitting with the Drude–Smith model [6, 17]. The energy band diagram of a 50 nm diameter SnO_2 NW shown in Fig. 2(b) was calculated via the self-consistent solution of the Poisson–Schrödinger equations in the effective mass approximation and cylindrical coordinates. Details of the self-consistent Poisson–Schrödinger (SCPS) solver are described in detail elsewhere [12]. The self-consistent potential profile of the SnO_2 NWs shown in Fig. 2(b) was determined by taking into account the effective mass of electrons $m_n^* = 0.2$ [13, 14] and relative dielectric permittivity $\varepsilon_r = 13.5$ of SnO_2 [15, 16].

We have also taken the Fermi level to be located ≈0.7 eV below the conduction band edge according to Kar et al. [11] who investigated the properties of SnO_2 NWs prepared by carbothermal reduction of SnO at 800 °C and found that the surface potential or barrier height was ≈0.65 eV. Based on the above we find that it is necessary to have a donor-like defect density of the order of 10^{18}–$10^{19}\,\mathrm{cm}^{-3}$ in order to obtain a one-dimensional electron gas (1DEG) line density

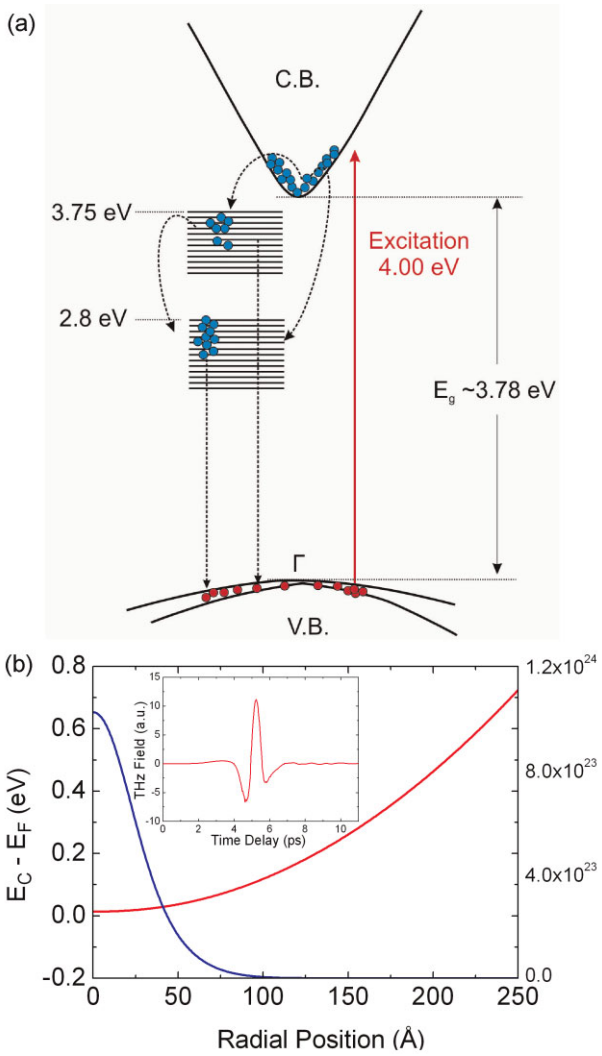

Figure 2 (online colour at: www.pss-a.com) (a) Energy band diagram depicting shallow and deep like defect states in SnO_2 NWs and carrier recombination pathways following excitation with 4.0 eV photons [5]. (b) SCPS conduction band edge potential profile with respect to the Fermi level (left axis) and 1DEG charge distribution (right axis) versus radial position. Inset shows temporal evolution of the THz *E*-field.

of $0.7 \times 10^9\,\mathrm{m}^{-1}$ which translates into a 3D density of $2.2 \times 10^{22}\,\mathrm{m}^{-3}$ by using the full cross-section. The CB edge potential is U-like and the electric field is zero *i.e.* a flat band condition exists at the core of the SnO_2 NW. The 1DEG charge distribution has a maximum at the core and decays to zero at a distance of 10 nm meaning that the depletion shell has a thickness of 15 nm. This is close to 18 nm obtained by Boyd and Brown [9] who take the barrier height to be 1.3 eV and find a carrier density of $10^{15}\,\mathrm{cm}^{-3}$ for a 60 nm diameter SnO_2 NW.

It should be noted that despite the large background density of positively charged donor-like states that are energetically located in the upper half of the band gap as

shown in Fig. 2(a) there are no 1D sub-bands below the Fermi level. The ground sub-band is at 40 meV above the Fermi level and the next one up at 97 meV giving a 'free' carrier density of the order of $10^{16}\,cm^{-3}$. Therefore the SnO_2 NWs are close to depletion. In fact, the SnO_2 NWs will be completely depleted for a donor-like density of $1 \times 10^{18}\,cm^{-3}$ due to the surface potential barrier of 0.7 eV and the positive charge of the donor-like states will be effectively counterbalanced by the negative charge located at the surface. Any perturbation of the surface charge and potential will therefore cause a dramatic change in the 1DEG density and the conductivity. More specifically a slight adsorption of negative ions will cause complete depletion whereas positive ions will gradually lower the surface potential and lead to a concomitant increase in the 1DEG density which makes SnO_2 NWs ideal for sensor applications [10].

4 Conclusions SnO_2 NWs with diameters of 50 nm and lengths $\leq$100 μm have been grown by low pressure reactive vapour transport via the reaction of Sn with O_2 at 800 °C. These have a tetragonal rutile crystal structure as confirmed by HRTEM, XRD. The free carrier density of the SnO_2 NWs was measured by THz absorption spectroscopy and was found to be $n = 3.3 \pm 0.4 \times 10^{16}\,cm^{-3}$ while the energetic position of the 1D sub-bands, overall band bending and charge distribution have been determined via the self-consistent solution of the Poisson–Schrödinger equations. We find that a high density of 10^{18}–$10^{19}\,cm^{-3}$ donor-like states located in the upper half of the energy band gap is required to obtain a free carrier density close to the measured value by taking the Fermi level to be situated ≈0.7 eV below the conduction band edge at the surface which gives a surface depletion shell thickness of 15 nm.

References

[1] M. Zervos, C. Karipi, and A. Othonos, Nanoscale Res. Lett. **7**, 175 (2012).
[2] P. Papageorgiou, M. Zervos, and A. Othonos, Nanoscale Res. Lett. **6**, 311 (2011).
[3] D. Tsokou, M. Zervos, and A. Othonos, J. Appl. Phys. **106**, 084307 (2009).
[4] A. Othonos, M. Zervos, and C. Christofides, J. Appl. Phys. **108**, 124302 (2010).
[5] A. Othonos, M. Zervos, and D. Tsokkou, Nanoscale Res. Lett. **4**, 828 (2009).
[6] D. Tsokkou, A. Othonos, and M. Zervos, Appl. Phys. Lett. **100**, 133101 (2012).
[7] M. Zervos, M. Demetriou, T. Krassia, and A. Othonos, RCS Adv. **2**, 4370 (2012).
[8] S. Ngamsinlapasathian, T. Sreethawong, Y. Suzuki, and S. Yoshikawa, Sol. Energy Mater. Sol. Cells **90**, 2129 (2006).
[9] E. J. Boyd and S. A. Brown, Nanotechnology **20**, 425201 (2009).
[10] E. Comini, Anal. Chim. Acta **568**, 28 (2006).
[11] A. Kar, M. A. Stroscio, M. Meyyappan, D. J. Gosztola, G. P. Wiederrecht, and M. Dutta, Nanotechnology **22**, 285709 (2011).
[12] M. Zervos and L. F. Feiner, J. Appl. Phys. **95**, 1 (2004).
[13] K. J. Button, D. G. Fonstad, and W. Dreybradt, Phys. Rev. B **4**, 4539 (1971).
[14] Y. Mi, H. Odaka, and S. Iwata, Jpn. J. Appl. Phys. **38**, 3453 (1999).
[15] H. J. van Daal, J. Appl. Phys. **39**, 4467 (1968).
[16] M. Batzill and U. Diebold, Prog. Surf. Sci. **79**, 47 (2005).
[17] N. V. Smith, Phys. Rev. B **64**, 155106 (2001).